MORPHOLOGY OF IONOSPHERIC SCINTILLATION*

R. K. Crane
Lincoln Laboratory, Massachusetts Institute of Technology
Lexington, Massachusetts

Abstract

Small scale ionospheric irregularities in the F-region can cause fluctuations in the amplitude, phase, and angle of arrival of VHF, UHF, and SHF signals traversing the ionosphere. Under some conditions, the power level fluctuations or scintillations at VHF and UHF may become severe with 12 dB signal level increases and fades in excess of 30 dB being observed. Current information about the probabilities of occurrence of severe fades is derived from a number of experiments using either radio star or satellite borne sources. The measurements are generally of signal level only and have been used to calculate scintillation indices to characterize scintillation intensity. An examination of the global distribution of scintillation indices show that scintillations are of importance to communication system performance primarily in the auroral and polar regions and at night near the geomagnetic equator.

I. Introduction

Early radioastronomical observations of sources of small angular extent exhibited significant intensity fluctuations. Spaced receiver measurements made at the Jodrell Bank Experiment Station[1] at 81.5 MHz showed that the intensity fluctuations originated in the F-region of the ionosphere, were correlated with the occurrence of spread-F, and formed a random intensity pattern on the ground with a correlation distance of approximately 4 km.

This paper is directed toward providing information to communication systems designers first about scintillation as observed in a single experiment, second about the adequacy of the existing models used to interpret scintillation data, and finally about the variation of scintillation with geophysical parameters. Scintillation due to electron density fluctuations has been observed on line-of-sight paths through the ionosphere at frequencies ranging from 20 MHz to 6 GHz. Frequencies between 100 and 400 MHz are emphasized in this paper because of their immediate concern in system design. An exhaustive literature exists on the subject of ionospheric scintillation. The references cited in this paper are not complete and are only intended to be illustrative. When possible the references will be to measurements made at frequencies in the 100 to 400 MHz range.

Prediction of fading statistics for the design of communication systems requires more than a cataloging of data from available observations. Most of the experimental data are from observations of limited duration for path geometries, frequencies, and locations different from the system to be designed. To obtain fading statistics for system design, either additional experiments must be made using precisely the frequency and path geometry of the proposed system or one of the diffraction or scintillation models must be used to interpret available data. The recent discovery of scintillation at 4 and 6 GHz in the equatorial region[2] was a surprise because it was not predicted using available data and the thin phase screen, Gaussian correlation function model.

Current knowledge of received signal fluctuations or scintillation caused by the ionosphere has been derived from a large number of observations of amplitude fluctuations made at meter, decimeter and centimeter wavelengths. The observations have been made over the past two decades at a number of locations using radio stars or satellite borne sources. The data have generally been recorded on strip charts. Various scintillation indices have been used to characterize the appearance of the recorded data on the charts. The scintillation indices were often subjectively estimated or, in recent years, calculated using the extreme values observed on short sections of the recording.[3] Information about the dependence of scintillation on geophysical parameters such as invariant latitude, magnetic activity index, and sunspot number has been published from summaries of the behavior of the qualitative scintillation index values compiled from available experimental data.[4-9]

Booker et al[10] proposed that diffraction by fluctuations of electron density in the ionosphere could cause the observed scintillation and that the effect of the electron density fluctuation could be modeled by a thin phase changing diffraction screen. Currently, scintillation phenomena are usually modeled as being caused by a thin screen using the refinements to the original analysis made by Mercier[11] and Briggs and Parkin.[12] The refinements included the introduction of a Gaussian spatial correlation function to describe the anisotropic fluctuations in electron density at and above the screen. Measurements of the spatial and temporal correlation properties of the fluctuations observed at the ground are often characterized by the scale size or correlation distance for the ionospheric diffraction screen using the Gaussian correlation function assumption.[13,14]

Recent observations have shown that the region of the ionosphere causing the fluctuations is often quite thick[15] and the thin screen model may not be adequate. The effects of random fluctuations of refractive index (or electron content) in a thick region may be analyzed using the Born (single

*This work has been sponsored by the Dept. of the Navy.

scattering) approximation to the wave equation[16] or the Rytov method (method of smooth perturbations)[17] when the scintillation index is not too large. In the limit of weak scintillation, all three approximate methods are identical. For strong scintillation, multiple scattering must be taken into account and none of the models are adequate.

II. Millstone Observations

Experiment Description

Observations of scintillation at 150 and 400 MHz were made during the period January 1971 to March 1973 using U.S. Navy Navigation System satellites and receivers at the Millstone Hill Radar Facility.[18] The satellites transmitted phase coherent signals which were simultaneously recorded at the receiver site. The UHF (400 MHz) receiver system included the 84-foot Millstone Hill antenna equipped for elevation and azimuth tracking and simultaneous observations using right and left hand circular polarization; a phase lock tracking receiver; and analog to digital conversion of the principal polarization channel AGC voltage, error channel signals, and the in-phase and quadrature orthogonal polarization channel voltages (referenced to the principal polarization signal). The data were samples at 15 times per second together with time, antenna pointing angle, and the VHF data and recorded on digital magnetic tape for post measurement analysis. The VHF receiver system provided in-phase and quadrature voltages for the 150 MHz signal referenced to the phase of the UHF signal divided down by the ratio of the frequencies. The VHF antenna was an eleven-element yagi mounted on one of the feed struts of the Millstone antenna.

The satellites were in circumpolar orbit at an approximate altitude of 1000 km and were tracked from horizon-to-horizon. For each pass the average signal levels at each frequency varied by about 10 dB. The VHF receiver system had a predetection bandwidth of approximately 250 Hz. The UHF predetection bandwidth was approximately 10 KHz and the AGC system had an effective bandwidth (closed loop) of 250 Hz. The signal to noise ratio for optimum observing conditions was approximately 35 dB at UHF and 25 dB at VHF. The receiver system was calibrated prior to each satellite pass.

Amplitude Fluctuations

Sample observations of received signal level at both frequencies are shown in Fig. 1. The data are for a pass during the most severe magnetic disturbance that occurred during the experiment (the planetary three hour magnetic activity index, Kp, equaled 8^+ at the time of the pass). The quiet conditions were observed to the south, the disturbed conditions through the auroral region to the north. Each 1/15 sec sample is displayed. Under quiet conditions, some fluctuations are

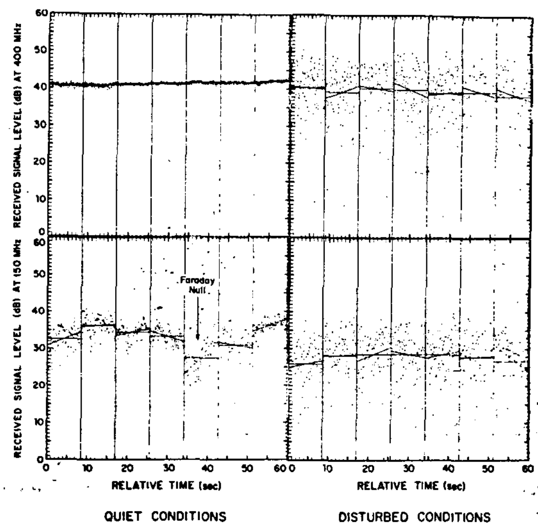

Figure 1.

observed at each frequency. Some of the variation at 150 MHz is also due to receiver noise. Faraday fading of the linearly polarized VHF signal is also evident as noted in the figure. Under disturbed conditions, peak-to-peak level changes of 45 dB at 400 MHz and 40 dB at 150 MHz are evident.

The data displayed in Fig. 1 are for roughly the same elevation angles, the mid-point elevation angle for the one minute quiet period was 7.6°; the mid-point elevation for the disturbed period was 8.1°. For lines-of-sight to the satellite at these elevation angles, the undisturbed signal levels should be identical for observations to the north and to the south of the receiver site. The detailed Faraday null structure of the 150 MHz signal will change, however, due to differences in the mean properties of the ionosphere. The sampled data were analyzed in overlapping 8.5 second intervals. The mean and linear least square fit line for the logarithm of the signal amplitude are displayed between the vertical lines for alternate analysis intervals. The short analysis intervals were chosen to best provide straight line fits to the variation in signal levels caused by the satellite, receiver geometry and Faraday fading at 150 MHz. The rms variation of the observed values about the least square lines were computed to characterize the intensity of the fluctuations. For each analysis interval and frequency, the rms variation of received power about a least square straight line fit to the observed power values was also calculated. The latter rms value, when normalized by the mean value of received power for the analysis interval is the S_4 index proposed by Briggs and Parkin.[12]

The values of S_4 for each analysis interval (with midpoints spaced by 4.3 sec) are displayed in Fig. 2 for the same satellite pass as for Fig. 1. The satellite rose in the south and the relatively

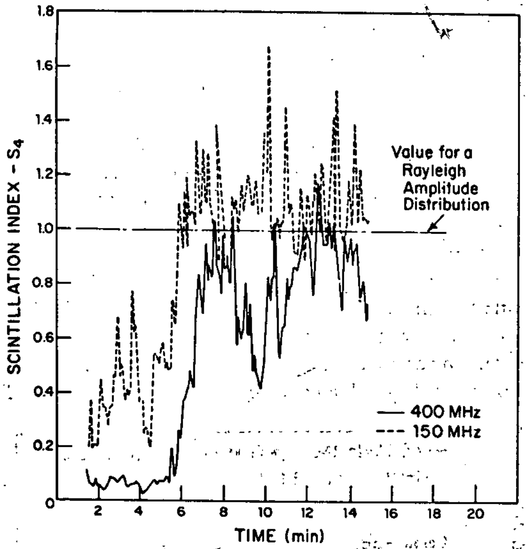

Figure 2

quiet conditions are evident for the first five minutes of the pass. Data for elevation angles below 2° are contaminated by tropospheric scintillation and surface multipath and are not displayed. The analysis of Briggs and Parkin indicates that $S_4 = 1$ is a limiting value for strong scintillations although values as high as 1.5 are possible for the right combination of scale size and distance from the thin screen. Although strong scintillation requires a consideration of multiple scattering, no analytical multiple scattering model is available. Experimental data both for ionospheric scintillation and tropospheric scintillation at optical frequencies[19] show that for strong scintillation or multiple scattering a limiting value is reached.

An obvious limiting value is shown in Fig. 3. This figure is a plot of the rms variation of the logarithm of the received signal, σ_χ, vs time for the same pass. In Fig. 3, the 95% confidence limits for the estimated error in calculating σ_χ are also depicted. The confidence limits are based upon the number of times different electron density irregularities are observed within the first Fresnel zone due to satellite motion. The data show that σ_χ reaches a limiting value of approximately 5.6 dB at each frequency. The limiting values depicted in Figs. 2 and 3 are calculated values for a Rayleigh received signal amplitude distribution. The spread of S_4 values about the limiting value of 1 at 150 MHz in Fig. 2 may be due either to sampling error or to a different signal amplitude distribution.

The empirical signal amplitude distributions for the two minutes depicted in Fig. 1 are shown in Fig. 4. The data show nearly identical distributions for the two frequencies and disturbed conditions. The UHF empirical distribution function appears to be log-normal for quiet conditions. Tropospheric scintillation at optical frequencies also appear to have a log-normal distribution in the limit of strong scintillation.[20] The distribu-

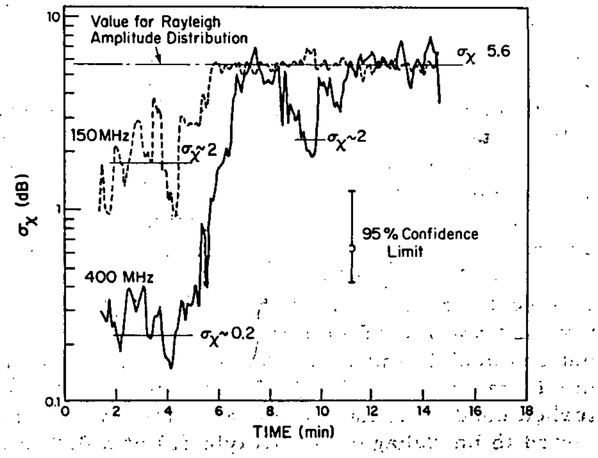

Figure 3

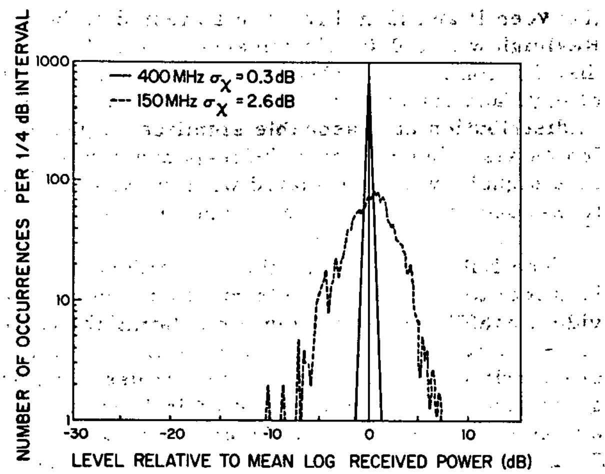

QUIET CONDITIONS

Figure 4a

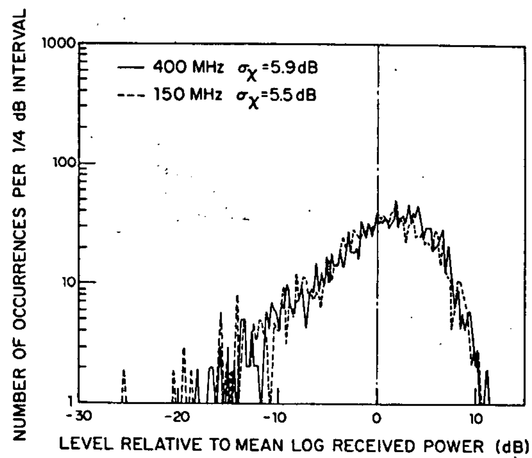

DISTURBED CONDITIONS

Figure 4b.

tion functions are, however, definitely not log-normal for ionospheric scintillation under disturbed conditions. Bischoff and Chytil[21] proposed the use of the Nakagami-m distribution as an approximation to the empirical distributions with

$m = 1/S_4^2$. Although the Nakagami-m distribution is not theoretically correct for the thin screen diffraction problem,[22] it may provide a reasonable approximate distribution and has been used for the construction of long term amplitude distribution functions.[23] The Nakagami-m distribution reduces to the Rayleigh distribution for $S_4 = 1$ and approaches the log-normal distribution for σ_χ less than 1 dB.[24] The empirical distribution functions depicted in Fig. 4 were tested against both the log-normal and Nakagami-m distributions for the calculated σ_χ values. Using the Pearson χ^2 distribution test and a 0.05 significance level, the distributions depicted in Fig. 4 were neither log-normal nor Nakagami-m. The VHF distribution for disturbed conditions had an m-parameter of 1.0 and tested to be Nakagami-m (Rayleigh) at a 0.01 significance level. The VHF distribution function for the minute preceding the disturbed minute (between 11 and 12 in Fig. 3) also tested as being Rayleigh with a 0.05 significance level. The UHF distribution for disturbed condition had an m-value of 0.92 and tested to be different from a Nakagami m distribution at reasonable significance levels. It was also observed that the in-phase and quadrature signals were correlated when m was not equal to one and were uncorrelated when m = 1.0.

The Nakagami-m distribution, although not identical to the observed distributions, does provide a useful approximation for relating the various forms of scintillation index used in the reduction of experimental data. Calculated values of S_4 and σ_χ for the satellite pass depicted in Figs. 2 and 3 are shown in Fig. 5. The relationship between S_4 and σ_χ calculated using both the Nakagami-m

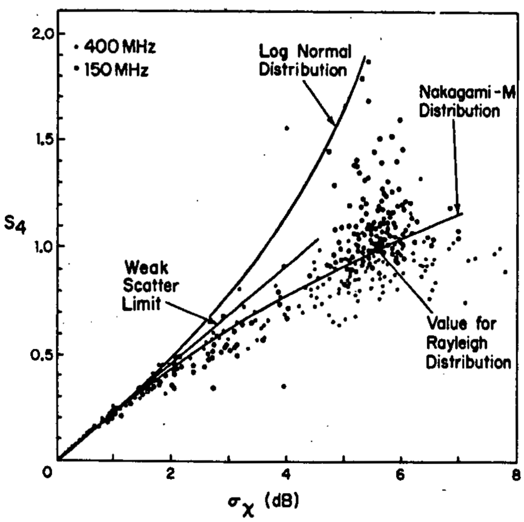

Figure 5

and log-normal distributions together with a weak scatter approximation are also shown. Of the distribution functions shown, the Nakagami-m provides the best estimate of the S_4-σ_χ relationship for the entire range of observed values. The usefulness of the Nakagami-m distribution for approximately relating the various signal variance values proposed by Briggs and Parkin and for relating the extreme value indices to other measures of scintillation is documented by Bischoff and Chytil.

The VHF amplitude fluctuations depicted in Fig. 1 appear to be more rapid for disturbed than for quiet conditions. The temporal behavior of scintillation can be quantitatively depicted by computing distributions of the time durations the signal is below or above present thresholds. Empirical distribution functions of duration below and above a level 3 dB below the mean log received power for each of the analysis intervals in the two minutes of data shown in Fig. 1 are presented in Fig. 6. The

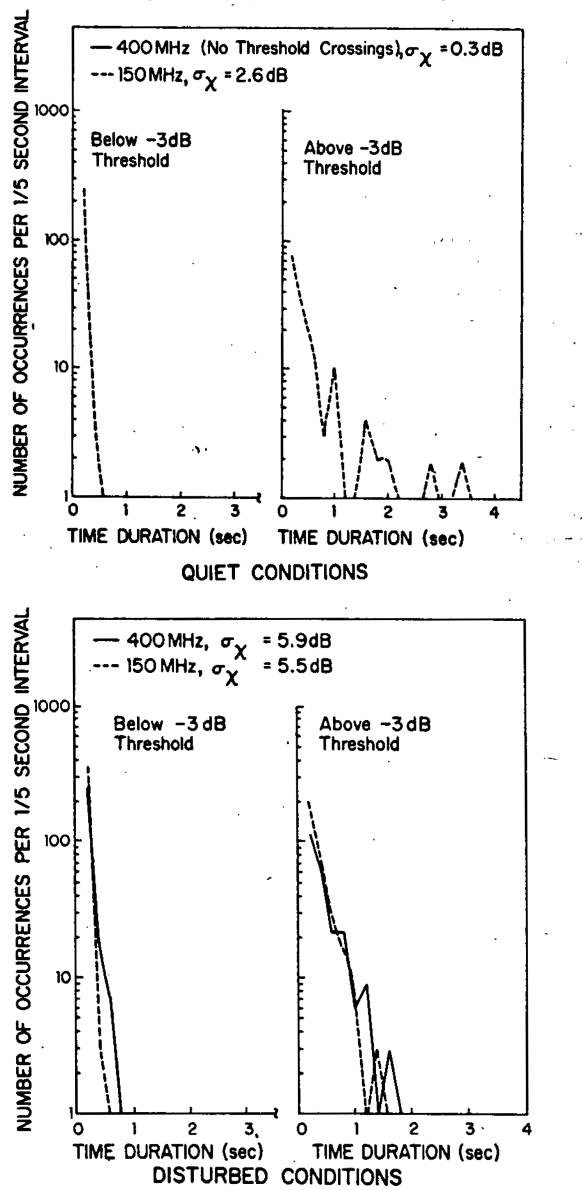

Figure 6

data show that the duration distribution functions are approximately exponential with different slopes for times above and below the -3 dB threshold. The average fade duration is given by the value of time duration required to reduce the number of observations by 1/e. For the -3 dB threshold and disturbed conditions, the average fade duration was 0.08 sec at 400 MHz and 0.05 sec at 150 MHz. The fade rate is the reciprocal of the average fade duration for a 0 dB threshold. For the quiet conditions depicted in Figs. 1 and 4, the fade rates were 3.8 Hz at UHF and 6.2 Hz at VHF. For disturbed conditions, the fade rates were higher being 7.2 Hz at UHF and 9.2 Hz at VHF.

The temporal behavior of scintillation may also be characterized by empirical correlation functions or power spectra. Power spectra for selected time periods from the pass depicted in Fig. 3 are displayed in Figs. 7 and 8. The power spectra were calculated using detrended log received power data from each analysis interval. The data for each interval were parabolically weighted prior to calculating the Fourier transform and the resultant power spectra were averaged over 13 analysis intervals within a minute. The resultant confidence limits for the power spectra estimates are shown in the figures. The spectra represent signal plus noise. The receiver noise levels are also depicted on each figure. The receiver bandwidths prior to sampling are approximately 250 Hz and with a sampling rate of only 15 per second (Nyquist frequency of 7.5 Hz) considerable aliasing is possible in the reported spectra.

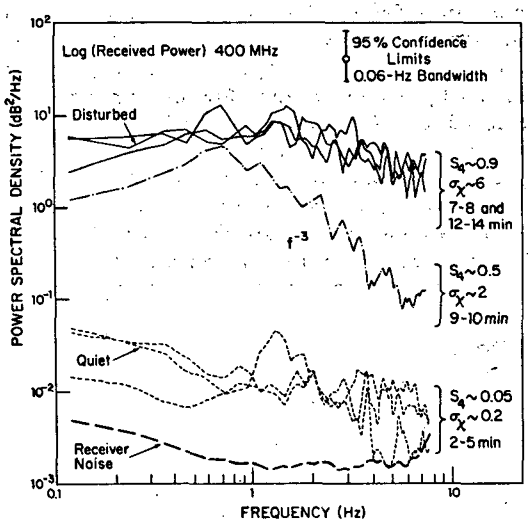

Figure 7

The UHF spectra for the quiet and disturbed times are identified on the figure. The dashed spectra are for minute intervals between 2 and 5 minutes as shown in Fig. 3. The horizontal lines with σ_χ values in Fig. 3 represent the duration spanned by the spectra displayed in Fig. 7. The dashed lines are for quiet or weak scintillation conditions. The quiet data are barely above receiver noise and are not useful in describing scintillation phenomena. The dot-dashed spectrum, for minute 9-10, is for a period when the strong scintillation limit was not reached. The spectra approximates a power law for frequencies greater than 1 Hz. Power law power spectra have been reported by Rufenach[25] and the power law form is evident in the data reported by Elkin and Papagiannis.[26] A line with a slope of -3 is drawn on the figure but the best fit slope for the power spectra may lie between -2 and -3. The fluctuations of the power spectra with frequency are due to the limited statistical accuracy of the reported values. One-minute sample sizes were chosen because the process is obviously not stationary over longer time intervals (except perhaps when the strong scintillation limit is reached as shown in Fig. 3) and may well not be stationary even over a minute. Shorter sample lengths were not chosen because the statistical error would become significantly larger.

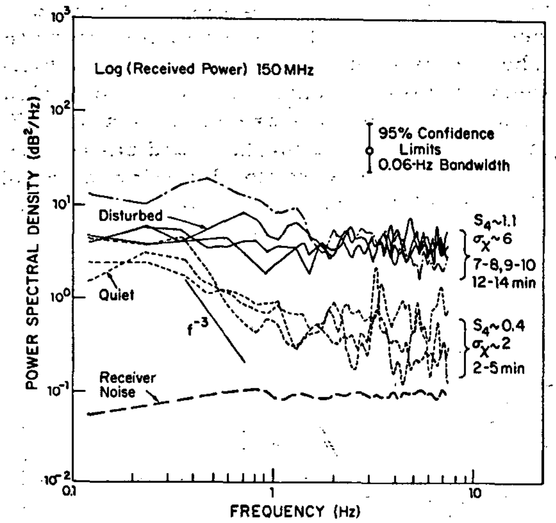

Figure 8

The spectra for disturbed or strong scintillation limit fluctuations are represented by solid lines. These data show little change of level with frequency implying that severe aliasing is present in the data and the sampling rate was not high enough to adequately represent the strong scattering case. The data were obtained as a part of a general propagation study and higher sampling rates would have compromised the other elements of the program. What is evident in the data is relatively little change in the low frequency variance energy and significant increases at higher frequencies. The correlation time therefore decreases and the spectrum spreads (fade rate increases) as the strong scintillation limit is reached. This result has been predicted heuristically by many workers.[12]

The VHF spectra for the disturbed period are also flat spectra. For quiet conditions, the σ_χ value is approximately the same as for the dot-dashed curve in Fig. 7. As in Fig. 7, the spectra at lower frequencies have almost the same levels as for the strong scintillation limit. For quiet conditions and frequencies above 1 Hz, the signal variance to noise variance ratios are not large enough to provide an adequate measure of the shape of each spectrum.

Phase Fluctuations

The phase of the signals from the satellite fluctuates when scintillation occurs. The differential phase path length was measured using the VHF in-phase and quadrature voltage values. The phase reference for the VHF signal was the phase of the UHF signal divided down by the ratio of the two frequencies. The differential phase path length values, reported in terms of phase change at 150 MHz reference the initially reported phase value, are shown in Fig. 9. The differential phase value at a sample instant is computed from the reported in-phase and quadrature voltage values and can only be determined modulo 2π. In processing the data, the assumption is made that the phase cannot change by more than π radians between successive samples. This assumption is adequate only if the data are samples at a sufficiently high rate. The in-phase and quadrature channel bandwidths were 250 Hz prior to sampling and it is possible that phase shifts greater than 2π can occur between sampling times.

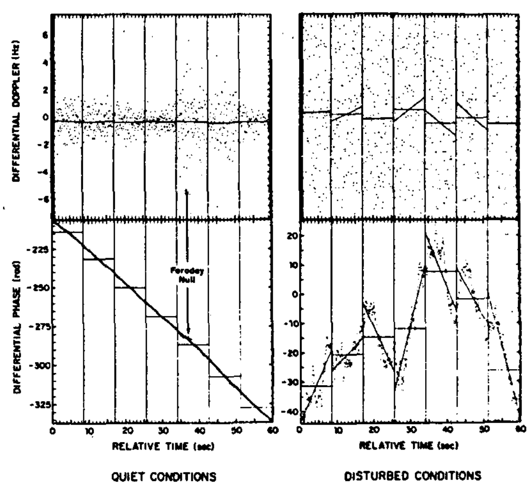

Figure 9

The differential doppler values for quite conditions (same observation times as for Fig. 1) show a relatively narrow spread of values about the origin suggesting that no phase ambiguity problems occurred. The differential phase values showed a smoothly changing trend caused by the change in integrated electron content along the path (see Garriott et al, 1970). The data show an increase in phase flucutations at the Faraday null cuased by a decrease in signal to noise ratio. The differential doppler data for disturbed conditions show a nearly uniform distribution of points between ± 7.5 Hz ($\pm\pi$ change between successive samples). For this data, occasional phase ambiguities are quite likely which introduce errors into the differential phase values. The low frequency differential phase fluctuations apparent in Fig. 9 for disturbed conditions may be due to actual changes in total electron content or to random inclusions of 2π radian phase ambiguities.

The rms variation in differential doppler and phase are depicted in Fig. 10 for the entire pass. The differential doppler values appear to show a strong scintillation limit at 4.3 Hz corresponding to the $\pi/\sqrt{3}$ rms value for phase change between successive observations of a Rayleigh process. The rms variations in differential phase show more uncertainty for strong scintillation due to possible phase ambiguities.

Power spectra for the differential phase fluctuation observations are shown in Fig. 11. The dashed curves correspond to weak scintillation and a sampling rate adequate to unambiguously measure differential phase. These power spectra show a region of generally linear (power law) decrease until the data are contaminated by receiver noise. For frequencies below .3 Hz the spectra are increasing with decreasing frequency though at a lower rate than for frequencies from .3-.6 Hz. The data at the low frequencies are, however, contaminated by the curve fitting, detrending procedure used to prepare the data for transform analysis. Phase difference power spectra observations reported by Porcello and Hughes[28] show reasonably convincing power law power spectra over a range from .1 to 10 Hz for satellites in orbits similar to those used for the Millstone measurements. The slopes of the power spectra observed by Porcello and Hughes ranged from -2.8 to -3.0. The strong scintillation data also show a power law behavior caused by the low frequency fluctuations evident in Fig. 9. This behavior however may be due to phase ambiguities and a higher sampling rate is required to adequately describe strong scintillation effects.

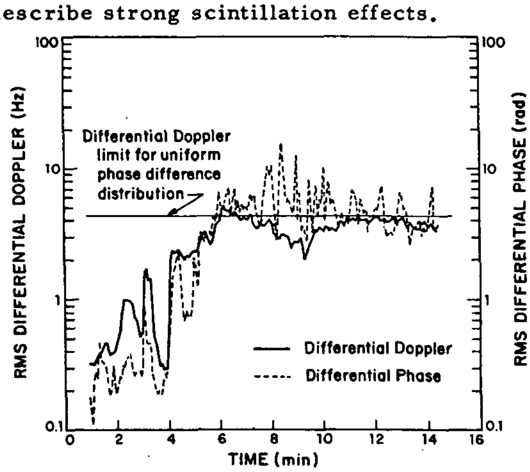

Figure 10

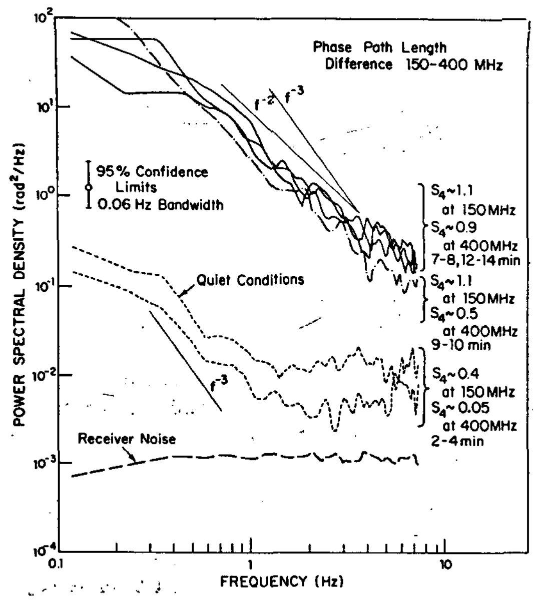

Figure 11

Depolarization

Simultaneous observations were made on both left and right hand circular polarizations at UHF. The transmissions were nominally right hand circular but in practice were elliptically polarized. The polarization state changed slowly with changes in satellite, receiver station geometry. The orthogonal polarization receiver was gain controlled by the primary polarization AGC signal. The AGC control system was effective in removing fluctuations of limited dynamic range that occurred simultaneously on both channels at frequencies up to 250 Hz. For strong fluctuations with peak-to-peak spreads of more than 20 dB, the AGC system did not remove all of the simultaneous fluctuations from the orthogonal channel output and the residual fluctuations were detected. For weak scintillation, only fluctuations on the orthogonal channel that were not correlated with the principal polarization fluctuations would be detected. For strong scintillation, the residual fluctuations had to be correlated with the principal polarization fluctuations to detect the presence or absence of uncorrelated fluctuations in the orthogonal polarization channel. The signal to noise ratio for uncorrelated fluctuations was in excess of 20 dB for typical satellite, receiver geometries.

The rms variation of the log of the orthogonal channel amplitude and the correlation coefficient between the log of the orthogonal channel output and the log of the principal channel output is shown in Fig. 12 for the entire pass (see Fig. 3 for principal polarization variation). For weak scintillation, the output is near receiver noise and no correlation is evident. After seven minutes, the scintillation is much stronger and a low level variation is evident in the orthogonal channel data. This residual output is however highly correlated with the scintillation in the principal polarization channel. The data therefore show no uncorrelated fluctuations.

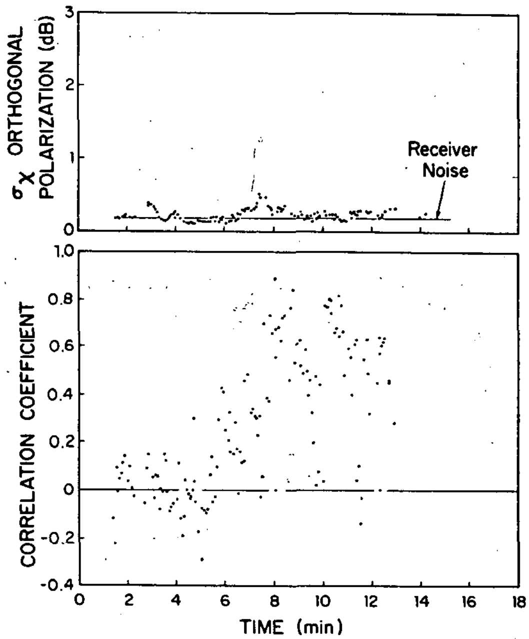

Figure 12

These observations show that the fluctuations on both polarizations are correlated and polarization diversity systems will not be useful in combating ionospheric scintillation at UHF. If significant uncorrelated orthogonal polarization fluctuations were present they would have a σ_X value near those in Fig. 3 which obviously were not observed in the data presented in Fig. 12 even for the strongest scintillation levels. Similar conclusions have been drawn by Whitney and Ring[29] from observations made at 137 MHz for scintillation levels below the strong scintillation limit and by Koster[30] for strong scintillation at 137 MHz in the equatorial region.

Observations at frequencies lower than 54 MHz show that orthogonal circular polarization channels may fade independently[31] and diversity is possible. At frequencies below about 50 MHz, the ordinary and extraordinary rays may be separated by more than the radius of the first Fresnel zone and the electron density fluctuations causing scintillation will not be correlated for two orthogonal polarizations.[32] Sufficient separation between ordinary and extraordinary ray paths for the fluctuations to become independent is not possible at frequencies above 100 MHz.

III. Carrier Frequency Dependence of the UHF, VHF Observations

Frequency Dependence of the Scintillation Index

The data presented above are provided to illustrate the characteristics of scintillation as observed at UHF and VHF. These data cna be used to provide information about scintillation at other locations, frequencies, and path geometries only if a model is available for their interpretation. In the limit of weak scintillation, the available models discussed above all relate the power spectrum of amplitude (or log amplitude) as observed on the ground to the power spectrum of the electron density fluctuations modified by the effects of the scattering process (Fresnel filtering). The power spectrum of temporal changes observed on a line-of-sight path to a low orbiting satellite may be related to the power spectrum of spatial fluctuations of electron density by assuming that the electron density fluctuations do not change during the time the line-of-sight sweeps through the disturbed region of the ionosphere.

Early models of scintillation assumed that the spatial correlation function for electron density fluctuations was approximately Gaussian with different scale sizes along and perpendicular to the magnetic field lines.[12] The Gaussian model implies a Gaussian power spectrum with power spectral densities decreasing rapidly for spatial frequencies above or below the reciprocal of the scale size. In the limit of high frequencies corresponding to spatial frequencies larger than the reciprocal of the Fresnel zone size, the spectrum observed on the ground should be identical to the two dimensional spectrum of electron density fluctuations observed in a plane normal to the direction of the propagation path. For a Gaussian model, the high frequency limit should have a parabolic shape with increasing negative slopes for increasing frequency when observed for weak scintillation. The dot-dashed curve in Fig. 7 has sufficient signal variation to noise variance ratio to show the slopes of the spectrum to be nearly linear shape for high frequencies is indicative of a power-law power spectrum rather than a Gaussian power spectrum.[25]

Power spectra at both UHF and VHF with a reasonably high signal variance to noise variance ratio and for weak scintillation are shown in Fig. 13. These spectra are for the same one minute observation periods and for a time period when the individual rms log amplitude values for each analysis interval changed little at both frequencies (the process was nearly stationary). Both spectra show power-law high frequency regions. The scintillation models predict that the power spectral density values should increase by the square of the ratio of the carrier wavelength. The best fit straight lines to both observed spectra having a wavelength squared separation are shown on the figure. The slope of these lines is approximately -3. This corresponds to a power law dependence for the three dimensional spatial power spectrum of electron density fluctuations with an index of 4 ($S \alpha k^{-p}$, S = power spectral density, k = wavenumber, p = index) and a one dimensional spectrum with an index of 2. The data presented in Fig. 13 are for observations to the northwest at an elevation angle of 18°. For the satellite, receiver station geometry, the Fresnel zone size at a height of 300 km was 0.7 km at 400 MHz and 1.1 km at 150 MHz. The ray moved at approximately 1.0 km/sec through the ionosphere (velocity perpendicular to the line-of-sight at 300 km). The frequency at which each of the spectra flatten (1.5 Hz at 400 MHz; 0.9 Hz at 150 MHz) is approximately the ratio of the ray motion to Fresnel zone size and higher frequencies correspond to scale sizes smaller than the Fresnel zone size.

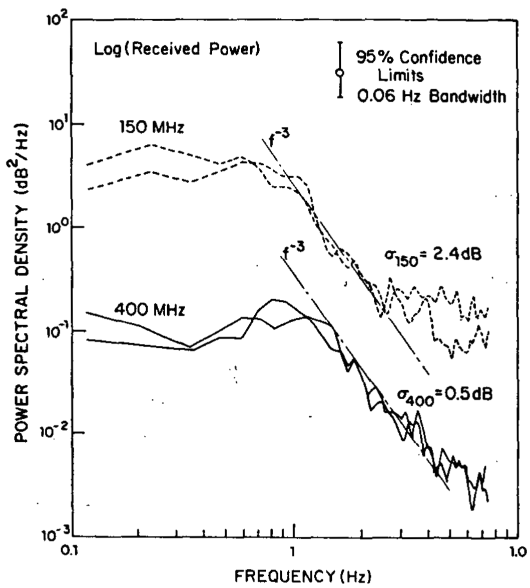

Figure 13

The weak scintillation theory for a power-law spectrum predicts a scintillation index (S_4 or σ_χ) frequency dependence given by[33]

$$\left(\frac{\sigma_{\chi_1}}{\sigma_{\chi_2}}\right) \alpha \left(\frac{\lambda_1}{\lambda_2}\right)^{(p+2)/4} = \left(\frac{\lambda_1}{\lambda_2}\right)^{\eta}$$

where λ is wavelength, the subscripts refer to the carrier frequencies, and η is the spectral index. For a three dimensional power-law index of 4, the spectral index is 1.5. Using this spectral index, σ_χ at 150 MHz should be 4.4 times σ_χ at 400 MHz. For the data displayed in Fig. 13, σ_χ at 400 MHz was 0.5 dB, σ_χ at 150 MHz was 2.4 2.4 dB, and the predicted value using η = 1.5 is 2.3 dB, well within the measurement error of the observed value. The relationship between σ_χ at 150 MHz and σ_χ at 400 MHz for a pass with reasonably high signal variance to noise variance ratios is shown on Fig. 14. The weak scintillation limit curve corresponding to a spectral index of 1.5 is shown together with the strong scintillation limit. The data appear to lie along the weak scintillation estimate curve until the strong scintillation limit is reached, then σ_X remains at the latter value.

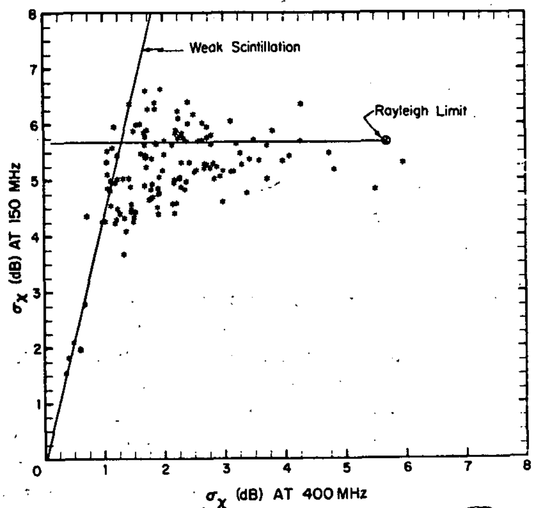

Figure 14

The frequency dependence of ionospheric scintillation has received considerably attention in the literature. The thin phase screen, Gaussian correlation function model predicted a spectral index of two when the scale size was larger than the first Fresnel zone radius (near field limit) and of one when the scale size was smaller (far field limit).[12] The power-law power spectra model predicts a single value for all cases (provided the power law holds over all scale sizes). Experimental verification of the frequency dependence predictions is difficult because the scintillation index must be less than the saturation limit value at both the high and low frequency. For strong scintillation at both frequencies, the empirically determined spectral index would be zero. For a random selection of observations, the empirical spectral index should lie between 0 and 1.5. Signal to noise and measurement dynamic range problems inherent in many of the early measurements could further degrade the estimates of spectral index. From Fig. 3 for the period between two and five minutes the ratio of σ_X values is approximately 10 implying a spectral index of 2.3. As shown in Fig. 8, the lower frequency was contaminated by receiver noise causing a fictitiously high spectral index estimate.

Simultaneous observations of radio star scintillation reported by Basu et al[34] showed a spectral index value of approximately 1.5 for frequencies at 112 and 224 MHz and a lower value for the 63, 112 MHz frequency pair. The lower value for the lower frequency presumably is caused by strong scintillation data. These observations were made at the Sagamore Hill Radio Observatory, less than 100 km from Millstone. Aarons[35] reported observations at frequencies between 22 and 39 MHz from Arecibo, Puerto Rico under weak scintillation conditions and found a median spectral index of 1.6. Amplitude scintillations observed by Lawrence et al[5] at 53 and 108 MHz show, for S_1 values at 53 MHz below 0.01 ($\sim S_4 = 0.7$), a median spectral index value of 1.5. Early observations reported by Chivers[36] made at Jodrell Band Experimental Station at several frequencies between 36 and 408 MHz using radio stars had mean spectral indices ranging from 1.9 to 2.1. Observations also made at Jodrell Bank at 79 and 1390 MHz and reported by Chivers and Davies[37] showed in the limit of weak scatter at 79 MHz and just detectable fluctuations at 1390 MHz, a value of η near 1.5.

Aarons et al[38] and Allen[39] argue, for observations made above 63 MHz from the Sagamore Hill Radio Observatory, that a spectral index of 2.0 best fits their data in the limit of weak scatter although the plots of scintillation index vs η curve have a median value of 1.6 as long as the scintillation index at 113 MHz is between 5 and 25% (S_4 at 63 MHz less than 0.6 and measurable scintillation at 113 MHz). Recently reported observations from the same observatory at frequencies of 137 and 412 MHz by Whitney et al[29] show, for similar weak but measurable scintillation conditions, a distribution of η values between 1.2 and 1.8 with a mean value of 1.49 ± 0.05.

Only a limited number of spectral index estimations have been made for equatorial regions. Blank and Golden[40] report $\eta \sim 0.2$ to 0.3 for frequencies between 137 and 400 MHz. They comment that the results pertain, in part, to strong scatter. Taur[41] reported a value of $\eta \sim 2$ for equatorial measurements at 4 and 6 GHz. The latter observations were for weak scintillation and may indicate either the existance of an inner scale where the power law region ends and a different power spectrum shape occurs or the problems of detecting small fluctuations in noise.

Correlation of Amplitude Fluctuations at Two Frequencies

The rms amplitude fluctuations decrease with increasing frequency for weak scatter. They are also correlated over a wide frequency range. Calculations of the expected correlation coefficient for power-law indices ranging from 3 to 4 are shown in Fig. 15. Similar calculations for Gaussian spectra have been made by Budden[42]. Since the available power spectra and frequency dependence data support the power law model, the Gaussian model predictions will not be presented. Measured correlation coefficients for the Millstone data and from available papers are also presented. The p = 4 curve provides the best estimate based upon the above analysis and should represent the upper bound for measurements for each Δf value. The lower frequencies used in the two frequency observations are listed in the figure. For strong scintillation, the correlation coefficient should be lower than the calculated values. For low frequency observations, the first Fresnel zones at each frequency may not overlap due to different ionospheric refraction at each frequency. For an elevation angle of 10°, rays at 150 and 400 MHz are separated by more than 30 km at a height of 300 km. The Millstone observations depicted in Fig. 1 show no correlation between the two frequencies. Since the elevation angles are less than 10° for the data depicted in Fig. 1 and the first Fresnel zone radii are less than 1.3 km, no correlation was expected.

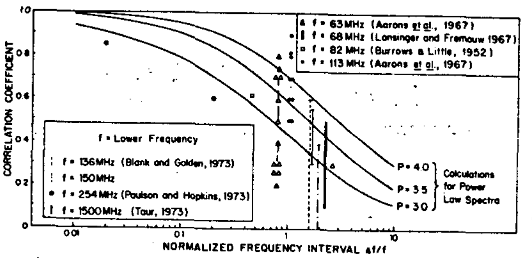

Figure 15

The data displayed on Fig. 15 show reasonable agreement with the calculations. The data reported by Taur[41] are the only data for weak scintillation only. These data with a lower frequency at 1550 MHz for an equatorial station shows better agreement for p between 3 and 3.5 than at 4. This again may indicate a change in the power spectrum of electron density fluctuations at small scale sizes in the equatorial region. The observations reported above for auroral and mid-latitude sites are all in reasonable agreement with a power-law power spectrum model with an index of 4 for the three dimensional fluctuations of electron density. The situation for equatorial regions is not as convincing and more data are required. It is, however, evident that the correlation coeffients are reasonably high over a wide frequency range. This implies that extremely wide frequency separations (~10 to 1) are required to provide adequate frequency diversity operation and frequency diversity is not useful in combating the effects of scintillation.

IV Dependence of Scintillation on Geophysical Parameters

Morphological studies of the dependence of scintillation on geophysical parameters have shown that scintillation is most severe and prevelent in and north of the auroral zone and near the geomagnetic equator (equatorial region within ± 15° to 20° of the geomagnetic equator). These studies of available scintillation observations show that the severity of scintillation also depends upon the elevation angle of the line-of-sight to the satellite, time of day, season of the year, the degree of magnetic disturbance, and sunspot number. In most of the observations, the exact nature of the dependance could not be determined due to the limited duration of the observations and possible correlations between some of the geophysical and geographical parameters. For observations of a radio star, the elevation angle and time of day are correlated for each season and the diurnal, elevation angle dependances cannot be separated. For observations of satellites in low circumpolar orbits, the effects of elevation angle and geomagnetic latitude cannot be separated without making simultaneous observations from a number of locations.[43]

Scintillations may be caused by electron density fluctuations anywhere in the ionosphere. Early studies showed strong correlation with the occurrence of spread-F and very weak correlation with sporadic E and spread E. This implies that the majority of scintillation occurrences are caused by F region irregularities. Studies of the heights of regions causing scintillation deduced from the rates of change of fluctuations observed using low orbiting satellites or from simultaneous observations at more than one station on the ground show that the electron density irregularities may occur over a wide range of heights, 200-600 km, both in the auroral and equatorial regions.[47,48,49] The radar data of Pomalaza et al[15] show that the irregularity region is usually several hundred kilometers thick.

Using the Rytov method to analyze weak scintillation due to a thick irregularity region, the variance of the log amplitude (σ_χ^2) is proportional to the integral of the product of the variance of the electron density fluctuations (intensity) and distance from the irregularities to the receiver over the thickness of the irregularity region for plane waves incident on the ionosphere and a three dimensional power law power spectrum with an index p = 4. The scintillation index, therefore, depends both upon the square root of the extent of the irregularity region along the line-of-sight path and to the square root of the distance from the receiver to the irregularity region. Both the distance to the irregularity region and the extent of the region along the ray vary with elevation angle. If the size intensity and location of the irregularity region are known, the scintillation index may be computed from the model for any combination of frequency and path geometry for σ_χ < 2-3 dB (weak scintillation). It is difficult however to deduce the intensity of the irregularities from observations using low orbiting satellites because the scintillation index value changes may be due to a change in size, a change of intensity, or a change in elevation angle.

The Millstone data for the satellite pass reported in Figs. 3 and 10 were replotted vs the invariant latitude of the line-of-sight to the satellite at a height of 300 km and are presented in Fig. 16. These data show a relatively rapid change from weak to strong scintillation as the variant latitude, Λ, changes from 56 to 59°. This sudden change may be described as a scintillation boundary in analogy with the boundary observed by Aarons et al[4]. The scintillation boundary considered by Aarons et al is defined as the latitude where their extreme value scintillation index, SI, exceeds 50% at 40 MHz. This translates to an S_4 value of 0.02 (σ_χ = 0.08 dB) at 400 MHz using a spectral index of 1.5 and the relationship between SI and S_4 reported by Bischoff and Chytil.[21] The 400 MHz observations made at Millstone do not have sufficient sensitivity to observe the boundary defined at 40 MHz although an apparent boundary is sometimes evident in the data. The abrupt changes in σ_χ and the apparent differences in σ_χ values to the north and south of Millstone (Λ = 56°) shown in Fig. 16 indicate changes in either the intensity or extent of electron density fluctuations with invariant latitude, the elevation angles being approximately the same for latitudes equispaced above and below 57° for the pass depicted in the figure. The data reported in Figs. 1 and 9 correspond to 51° and 64° for quiet and disturbed conditions to the north and south of the boundary, respectively.

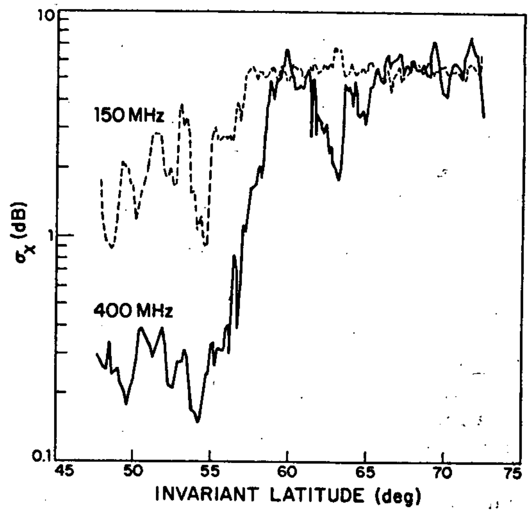

Figure 16

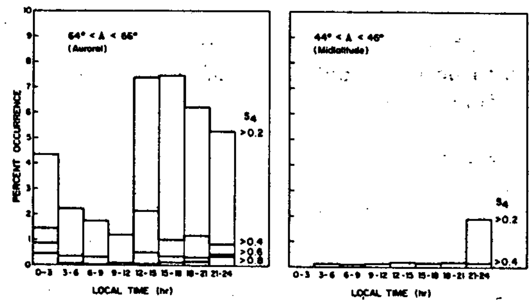

Figure 17

Auroral and mid-latitude scintillation regions are separated by the scintillation boundary. The position of the boundary changes with time of day, magnetic activity, and possibly sunspot number. Aarons[50] reported that the position of the boundary defined using the mean SI values for a number of observations ranged from 54° to 76° depending upon time of day and magnetic activity. The diurnal variation of S_4 at 400 MHz tabulated from Millstone data for detrended three-second observation periods[51] are shown in Fig. 17 Two invariant latitude bands were analyzed, 44 to 46° corresponding to positions always within the mid-latitude region (south of the boundary) and 64 to 66° corresponding to locations within the night time auroral region. Data from a total of 2471 passes were analyzed. For the two-invariant latitude bands used, the elevation angles ranged from 3° to 14°. The elevation angle values for each pass however were generally different in each band. Over the range of elevation angles, the S_4 or σ_χ value may change by a factor of 2. The elevation angles should have nearly the same occurrence distribution for each band and no elevation angle bias is expected.

The occurrence percentages of S_4 values above 0.2, 0.4, 0.6 and 0.8 (σ_χ values of 0.9, 1.8, 2.8 and 4.2 dB, respectively) were chosen to characterize the observations. For S_4 > 0.8, the 64-66° data show a morning minimum and an afternoon maximum. Data reported by Aarons[50] for Narssarssuaq having an invariant latitude of 63° and an elevation angle of 18° show, at 136 MHz, a morning minimum in mean SI and a nighttime maximum occurring between 2100 and 0500 hours. The Millstone afternoon maximum is not evident in the 136 MHz data. Aarons et al[4] reported occurrence percentages for SI > 60% at 136 MHz (equivalent to S_4 > 0.15 at 400 MHz) that displayed a morning minimum and a nighttime maximum. Although the Narssarssuaq data are for nearly the same invariant latitude as the Millstone data and the elevation angles differ slightly, the latter data show an afternoon maximum not present in the former. The Millstone data are for observations to the north, the Narssarssuaq data for observations toward the south and differences in propagation direction relative to the field lines might be important. 113 MHz data reported by Aarons[50] for radio star observations toward the North at an invariant latitude of 66° at the same elevation angles as for Millstone show relatively higher mean SI values in the afternoon than in the morning displaying the same general trend as the Millstone data. The 113 MHz data also showed a lower mean SI value averaged over all times of day than the 136 MHz data. The lower SI values are presumably due to differences in sunspot number, the 113 MHz data were taken at the minimum of the sunspot cycle; the 136 MHz and Millstone data near the maximum. The shape of the diurnal variation curves may be affected by differences in the intensity and extent of the irregularities along and normal to the field lines.

The mid-latitude region observations show significantly smaller percentages of occurrence for each of the three hour intervals. The number of satellite passes associated with the observed occurrences with $S_4 > 0.2$ range between 0 and 2 for all intervals except 2100-2400 hours implying that insufficient data were available to deduce a diurnal trend. Mid-latitude observations by Aarons et al[52] at 54 MHz show mean SI values to have relative maxima at noon and midnight. Equatorial region observations show scintillation to be a nighttime phenomena with occurrences rare between sunrise and sunset.[9] Observations reported by Aarons et al[4] for Huancayo, Peru (equatorial) show that at 136 MHz the scintillations were most prevelent at 2200 h. local time with a 60% occurrence for SI > 60. This translates to a 60% occurrence of $S_4 > 0.15$ at 400 MHz. The data in Fig. 17 show less than 10% occurrence for $S_4 > 0.2$ indicating that equatorial scintillations tend to be more prevalent than auroral zone scintillations.

The seasonal dependence of scintillation is shown for the Millstone mid-latitude and auroral region observations in Fig. 18. These data show a spring minimum and a fall maximum for the auroral data at $S_4 > 0.2$. The August peak is caused by a three day interval associated with the highest magnetic activity indices observed during the January 1971 to March 1973 time period. The August event biases the observations. The seasonal variation of mean SI at 54 MHz reported by Aarons et al[52] show a minimum in the number of occurrences in Winter as compared to other seasons for all observations to the north and south of the Sagamore Hill Observatory. The 54 MHz data are however for the minimum of the sunspot cycle. The data, therefore, show little real seasonal variation. Equatorial region observations tend to show relatively higher percentage occurrences at the times of the equinoxes and a minimum at the northern solstice.

Observations of scintillation in the auroral region generally show a correlation between mean SI values and magnetic activity, Kp. Figure 19 shows the increase in the occurrence of scintillation with increasing Kp for the auroral region. Little change in percentage occurrences of $S_c > 0.2$ is noted for the mid-latitude region. Aarons[52] noted that the position of the scintillation boundary is correlated with Kp, moving south as Kp increases. In contrast to the apparent dependence of scintillation on magnetic activity in the auroral region, Koster[9] notes that scintillation in the equatorial region is suppressed during periods of enhanced magnetic activity. These results may vary with the sunspot cycle but insufficient data are available to test dependences on sunspot numbers. Available long term observations of scintillation over a significant part of the sunspot cycle have only shown that scintillation tends to be both more prevalent and more intense on average during years of high sunspot n'.mber.

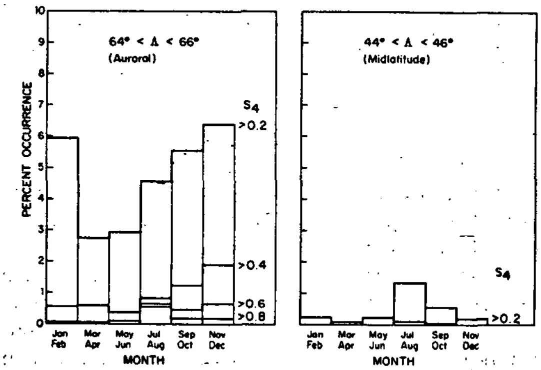

Figure 18

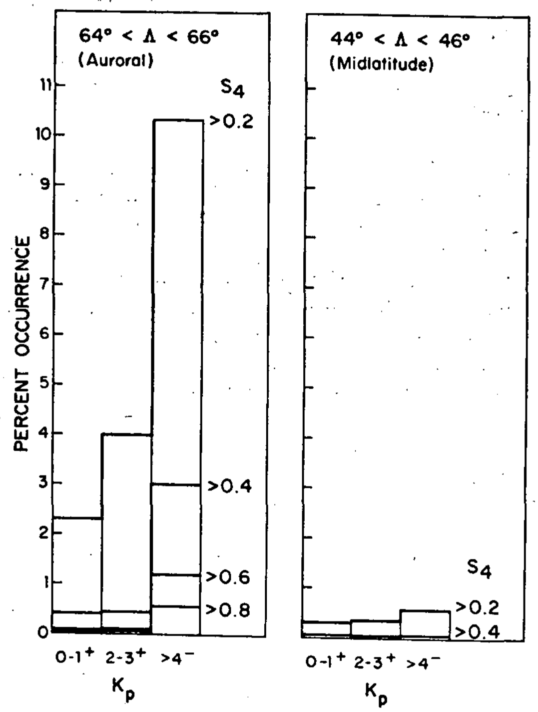

Figure 19

V. Conclusions

The statistical summary of the Millstone data show a clear dependence upon magnetic activity although diurnal and seasonal variations are not well defined. The data are, however, for a relatively short time period when compared with the sunspot cycle and are, therefore, not complete enough to provide an empirical model for the prediction of scintillation statistics for use in communication system design. To provide the required statistics, data from a large number of observations spread over at least half a sunspot cycle are required. Other available observations have generally been made at frequencies below 137 MHz and are only useful for the prediction of scintillation at lower frequencies due to the limiting effect of strong scintillation.

The auroral region observations clearly show that scintillation will affect system design at frequencies up to at least 400 MHz. The equatorial region observations of Taur[2] show frequencies up to 6 GHz are affected. Since scintillation is a fact of life at UHF and VHF what methods can be used to mitigate its effects? While the data are somewhat inadequate, some recommendations can be made. First, some negative recommendations: The two frequency correlation function analysis showed that scintillation is a wideband phenomena and frequency diversity is not practical. The cross polarization observations showed that scintillations on the principal and orthogonal circular polarizations were correlated implying that polarization diversity will not work at UHF. While these analyses and measurements were performed for auroral region observations, we believe the results also apply in the equatorial region. For the auroral region, the weak scintillation data showed power law power spectra for electron density irregularities. Preliminary analysis of 254 MHz data reported for the equatorial region[46] also show power law spectra (with a three-dimensional index p = 4). This suggests that although the mechanisms causing equatorial region irregularities may be different from those active in the auroral region, the resultant effects of the irregularities on propagation are the same and the results obtained from the Millstone data apply in the equatorial region.

One possible solution is space diversity: The Millstone observations were taken using a low orbiting satellite. The temporal variation of the signal level is caused by the motion of the line-of-sight through the irregularities. The satellite motion is known, hence the temporal variations may be interpreted in terms of the spatial variation of electron density. The frequency scale on Fig. 13 may be interpreted as a wavenumber scale with, for the satellite, receiver geometry pertinent to Fig. 13, the 1 Hz value equivalent to $2\pi\ km^{-1}$ (scale size of 1 km). Since the width of each power spectrum is approximately the reciprocal of the correlation distance, the correlation distance is approximately 0.5 km at UHF and 0.8 km at VHF. This implies that the scintillation observed at receivers spaced by more than the correlation distance (~ Fresnel zone size) should be uncorrelated and could be combined to get diversity. For strong scintillation, the power spectrum broadened implying that smaller diversity distances may be useful in that limit.

Another possible solution is time diversity: The fade duration statistics reported above reflect the motion of the line-of-sight through the medium and, for weak scintillation the duration values should be inversely proportional to the translation velocity of the ray at the height of the irregularities. For geostationary satellites, the line-of-sight is fixed and the irregularities drift by. The fade duration values then should be inversely proportional to the drift rate. Using a 100 m/sec drift rate as typical[4] the fade durations should be an order of magnitude larger than those shown in Fig. 6. For strong scintillation, the fade durations should be shorter than for weak scintillation as shown in the discussion of Fig. 6 The power spectra shown in Fig. 13 imply a correlation time the order of 0.5 sec at UHF and 0.8 sec at VHF. As with the fade duration values, the correlation time is dependent upon the velocity of the irregularities perpendicular to the line-of-sight. Since the signal becomes uncorrelated in time, time diversity is also possible. For geostationary satellites, correlation time depends both on the Fresnel zone size and the drift velocity of the irregularities. The latter is a random variable that has to be observed at many locations over a long period of time to provide an adequate statistical description. Since the fade rate or correlation time is different for strong scintillation, observations must be made in the weak scintillation regime to define drift velocities.

VI. Recommendations

The only solutions we have recommended are the use of space of time diversity. Some guidelines for their application may be obtained from Millstone and other available data. However, to optimize system deisgn, more information is required. We recommend:

1. Additional available weak scintillation data should be processed to determine the structure of the power spectrum to establish if the power law form represents all observations.

2. Available weak scintillation data from geostationary satellite observations should be analyzed to determine drift rate statistics.

3. New observations using both low-orbiting and geostationary satellites with several coherently related carrier frequencies widely spread in the UHF, SHF band at and above the frequencies of interest should be made to provide adequate statistics of amplitude, phase, and drift velocity. The

frequencies should be chosen such that weak scintillation is always observed at one of the frequencies.

Acknowledgment

The author acknowledges the help and support of Drs. J. V. Evans and R. H. Wand of the Millstone Hill radar site in making their data available for analysis and of T. M. Turbett for the data processing. The percentage occurrance data used in preparing Figs. 17 to 19 were provided by Dr. Wand.

References

1. C. G. Little and A. Maxwell, "Fluctuations in the Intensity of Radio Waves from Galactic Sources," Phil. Mag. 42 267-278 (1951).

2. R. R. Taur, "Ionospheric Scintillation at 4 and 6 GHz," COMSAT Tech. Rev. 3 145-163 (1973a).

3. H. E. Whitney, J. Aarons, and C. Malik, "A Proposed Index for Measuring Ionospheric Scintillations," Planet. Space Sci. 17 1069-1073 (1969).

4. J. Aarons, H. E. Whitney, and R. S. Allen, "Global Morphology of Ionospheric Scintillations," Proc. IEEE 59 159-172 (1971).

5. R. S. Lawrence, J. L. Jespersen, and R. C. Lamb, "Amplitude and Angular Scintillations of the Radio Source Cygnus-A Observed at Boulder, Colorado," J. of Res. NBS 65D 333-350 (1961).

6. G. S. Kent, "High Frequency Fading of the 108 Mc/s Wave Radiated From an Artificial Earth Satellite as Observed at an Equatorial Station," J. Atmosph. Terr. Phys. 22 255-269 (1961).

7. C. G. Little, G. F. Reid, E. Stiltner, and R. P. Merritt, "An Experimental Investigation of the Scintillation of Radio Stars Observed at Frequencies of 223 and 456 Mega cycles per Second from a Location Close to the Auroral Zone," J. Geophys. Res. 67 1763-1784 (1962).

8. E. J. Fremouw and H. F. Bates, "World-wide Behavior of Average VHF-UHF Scintillation," Radio Sci. 6 863-869 (1971).

9. J. R. Koster, "Equatorial Scintillation," Planet. Space Sci. 20 1999-2014 (1972).

10. H. G. Booker, J. A. Ratcliffe, and D. H. Shinn, "Diffraction from an Ionospheric Screen with Application to Ionospheric Problems," Phil. Tran. Roy. Soc. A242 579-607 (1950).

11. R. P. Mercier, "Diffraction by a Screen Causing Large Random Phase Fluctuations," Proc. Camb. Phil. Soc. 58 382-400 (1962).

12. B. H. Briggs and I. A. Parkin, "On the Variation of Radio Star and Satellite Scintillations with Zenith Angle," J. Atmosph. and Terr. Phys. 25 339-365 (1963).

13. J. R. Koster, "Ionospheric Studies Using the Tracking Beacon on the 'Early Bird' Synchronour Satellite," Ann. de Geophys. 22 103-107 (1966).

14. J. Pomalaza, R. F. Woodman, G. Tisnado, J. Sandoval and A. Guillev, "A Progress Report on Scintillation Observations at Ancon and Jicamarco Observatories," NASA/GSFC X-520-70-398 NASA Goddard Space Flight Center, Greenbelt, Md. (October 1970).

15. J. Pomalaza, R. F. Woodman, J. Tisnado, and E. Nakasone, "Study of Equatorial Scintillations, A Progress Report," NASA/GSFC X-750-73-244, NASA Goddard Space Flight Center, Greenbelt, Md. (December 1972).

16. K. G. Budden, "The Amplitude Fluctuations of the Radio Wave Scattered from a Thick Ionospheric Layer with Weak Irregularities," J. Atmosph. and Terr. Phys. 27 155-172 (1965).

17. V. I. Tatarskii, The Effects of the Turbulent Atmosphere on Wave Propagation, Nauka, Moscow, 1967; Trans. avail. U.S. Dept. of Comm. National Technical Information Service, Springfield, Va.

18. J. C. Gilhoni, ed. "Millstone Radar Propagation Study: Radar Instrumentation," Technical Report 507, Lincoln Laboratory, MIT (In press, 1973).

19. G. R. Ochs and R. S. Lawrence, "Saturation of Laser-Beam Scintillation Under Conditions of Strong Atmospheric Turbulence," J. Optical Soc. Amer. 59 226-227 (1969).

20. J. R. Dunphy and J. R. Kerr, "Scintillation Measurements for Large Integrated-Path Turbulence," J. Optical Soc. Amer. 63 981-986 (1973).

21. K. Bischoff and B. Chytil, "A Note on Scintillation Indices, " Planet, Space Sci. 17 1059-1066 (1969).

22. C. L. Rino and E. J. Fremouw, "Statistics for Ionospherically Diffracted UHF/VHF Signals," Radio Sci. 8 223-233 (1973).

23. H. E. Whitney, J. Aarons, R. S. Allen and D. R. Seemann, "Estimation of the Cumulative Amplitude Probability Distribution Function of Ionospheric Scintillation," Radio Sci. 7 1095-1104 (1972).

24. M. Nakagami, "The m-distribution--A General Formula of Intensity Distribution of Rapid Fading," in Statistical Methods on Radio Wave Propagation, ed. W. C. Hoffman, (Pergamon Press, New York, 1960).

25. C. L. Rufenach, "Power-Law Wavenumber Spectrum Deduced from Ionospheric Scintillation Observations," J. Geophys. Res. 77 4761-4772 (1972).

26. T. J. Elkins and M. D. Papagiannis, "Measurement and Interpretation of Power Spectrums of Ionospheric Scintillation at a Sub-auroral Location," J. Geophys. Res. 74 4105-4115 (1969).

27. O. K. Garriott, A. V. daRosa, "Electron Content Obtained from Faraday Rotation with Phase Length Variations," J. Atmosph. and Terr. Phys. 32 705-727 (1970).

28. L. J. Porcello and L. R. Hughes, "Observed Fine Structure of a Phase Perturbation Induced During Transauroral Propagation," J. Geophys. Res. 73 6337-6346 (1968).

29. H. E. Whitney and W. F. Ring, "Dependency of Scintillation Fading of Oppositely Polarized VHFSignals," IEEE Trans. Antennas and Propagat. AP-19 (1971).

30. J. R. Koster, "Ionospheric Studies Using the Tracking Beacon on the 'Early Bird' Synchronous Satellite," Ann. de Geophys. 22 435-439 (1966).

31. J. P. McClure, "Polarization Measurements During Scintillation of Radio Signals from Satellites," J. Atmosph. and Terr. Phys. 27 335-348 (1965).

32. R. S. Roger, "The Effect of Scintillations on the Polarization of Satellite Transmissions near 20 Mc/s," J. Atmosph. and Terr. Phys. 27 335-248 (1965).

33. A. T. Young, "Interpretation of Interplanetary Scintillations," Astrophys. J. 168 543-562 (1971).

34. S. Basu, R. S. Allen, and J. Aarons, "A Detailed Study of a Brief Period of Radio Star and Satellite Scintillations," J. Atmosph. and Terr. Phys. 26 811-823 (1964).

35. J. Aarons, "Ionospheric Irregularities at Arecibo, Puerto Rico," J. Atmosph. and Terr. Phys. 29 1619-1624 (1967).

36. H. J. A. Chivers, "The Simultaneous Observation of Radio Star Scintillations on Different Radio-Frequencies," J. Atmosph. and Terr. Phys. 17 181-187 (1960).

37. H. J. A. Chivers and R. D. Davies, "A Comparison of Radio Star Scintillations at 1390 and 79 Mc/s at Low Angles of Elevation," J. Atmosph. and Terr. Phys. 24 573-584 (1962).

38. J. Aarons, R. S. Allen, and T. J. Elkins, "Frequency Dependence of Radio Star Scintillations," J. Geophys. Res. 72 2891-2902 (1967).

39. R. S. Allen, "Comparison of Scintillation Depths of Radio Star and Satellite Scintillations," J. Atmosph. and Terr. Phys. 31 289-297 (1969).

40. H. A. Blank and T. S. Golden, "Analysis of VHF/UHF Frequency Dependence, Space, and Polarization Properties of Ionospheric Scintillation in the Equatorial Region," 1973 IEEE Inter. Comm. Conf. Proc. 17-27 to 17-35, (June 1973).

41. R. R. Taur, Private Communication (1973).

42. K. G. Budden, "The Theory of the Correlation of Amplitude Fluctuations of Radio Signals at Two Frequencies, Simultaneously Scattered by the Ionosphere," J. Atmosph. and Terr. Phys. 27 883-897 (1965).

43. Joint Satellite Studies Group, "On the Latitude Variation of Scintillations of Ionospheric Origin in Satellite Signals," Planet. Space Sci. 16 775-781 (1968).

44. J. M. Lansinger and E. J. Fremouw, "The Scale Size of Scintillation Producing Irregularities in the Auroral Ionosphere," J. Atmosph. and Terr. Phys. 29 1229-1242 (1967).

45. K. Burrows, and C. G. Little, "Simultaneous Observations of Radio Star Scintillations on Two Widely Spaced Frequencies," Jodrell Bank Ann. 1 29-35 (1952).

46. M. R. Paulson and R. V. F. Hopkins, "Effects of Equatorial Scintillation Fading on Satcom Signals," NELC/TR 1875, Naval Electronics Laboratory Center, San Diego, Calif. (May 1973).

47. J. Frihagen and L. Liszha, 'A Study of Auroral Zone Ionospheric Irregularities Made Simultaneously at Tromso, Norway and Kirana, Sweden, J. Atmosph. and Terr. Phys. 27 513-523 (1965).

48. J. L. Jesperson and G. Kamas, "Satellite Scintillation Observations at Boulder, Colo.," J. Atmosph. and Terr. Phys. 26 457-473 (1964).

49. R. F. Kelleher and J. Sinclair, "Some Properties of Ionospheric Irregularities as Deduced from Recordings of the San Marco II and BE-B Satellites," J. Atmosph. and Terr. Phys. 32 1259-1271 (1970).

50. J. Aarons, "A Descriptive Model of F-Layer High-Latitude Irregularities as Shown by Scintillation Observations," J. Geophys. Res. 78 7441-7450 (1973).

51. J. V. Evans, ed., "Millstone Radar Propagation Study: Scientific Results," Technical Report 509, Lincoln Laboratory, MIT (In press, 1973).

52. J. A. Aarons, J. Mullan, and S. Basu, "The Statistics of Satellite Scintillations at a Subauroral Latitude," J. Geophys. Res. 69 1785-1794 (1964).

List of Illustrations

Fig. 1 UHF and VHF amplitude measurements obtained from a pass of Object #3133 on 4 August 1972.

Fig. 2 S_4 vs time for pass of Object #3133 rising at 0411 GMT on 4 August 1972 ($Kp = 8^+$).

Fig. 3 σ_χ vs time for pass of Object #3133 rising at 0411 GMT on 4 August 1972 ($Kp = 8^+$).

Fig. 4 Empirical amplitude distribution functions for data shown in Fig. 1.

Fig. 5 S_4 vs σ_χ for pass of Object #3133 rising at 0411 GMT on 4 August 1972 ($Kp = 8^+$).

Fig. 6 Empirical distribution functions for durations below and above a -3 dB threshold relative to the mean log received power for the data shown in Fig. 1.

Fig. 7 UHF log amplitude power spectra for selected minutes from the pass of Object #3133 rising at 0411 GMT on 4 August 1972 ($Kp = 8^+$).

Fig. 8 VHF log amplitude power spectra for selected minutes from the pass of Object #3133 rising at 0411 GMT on 4 August 1972 ($Kp = 8^+$).

Fig. 9 Differential phase and differential doppler measurements obtained from a pass of Object #3133 on 4 Aug. 1972.

Fig. 10 Rms variations in differential phase and differential doppler for pass of Object #3133 rising at 0411 GMT on 4 August 1972 ($Kp = 8^+$).

Fig. 11 Differential phase power spectra for selected minutes from the pass of Object #3133 rising at 0411 GMT on 4 August 1972 ($Kp = 8^+$).

Fig. 12 Rms variation in the output from the orthogonally polarized channel and correlation coefficients between the principal and orthogonal channel outputs for pass of Object #3133 rising at 0411 GMT on 4 August 1972 ($Kp = 8^+$).

Fig. 13 Power spectra for log received power fluctuations at both UHF and VHF for the same one minute observation period of the pass of Object #3133, 5 August 1972 at 0334 GMT ($Kp = 8^+$).

Fig. 14 Rms variation of log received power at VHF vs simultaneously observed value at UHF from pass of Object #3133 rising at 2342 GMT on 4 August 1972 ($Kp = 8^+$).

Fig. 15 Two frequency correlation functions for amplitude fluctuations.

Fig. 16 Latitude dependence of scintillation for pass of Object #3133 rising at 0411 GMT 4 August 1972 ($Kp = 8^+$).

Fig. 17 Diurnal variation of scintillation at 400 MHz for auroral and mid-latitudes for 2471 satellite passes observed between January 1971 and March 1973.

Fig. 18 Seasonal variation of scintillation at 400 MHz for auroral and mid-latitudes for 2471 satellite passes observed between January 1971 and March 1973.

Fig. 19 Magnetic activity dependence of scintillation at 400 MHz for auroral and mid-latitude for 2471 satellite passes observed between January 1971 and March 1973.